# Complementary Roles of Whole-Body Diffusion-Weighted MRI and $^{18}$F-FDG PET: The State of the Art and Potential Applications

Thomas C. Kwee[1], Taro Takahara[1], Reiji Ochiai[2], Dow-Mu Koh[3], Yoshiharu Ohno[4], Katsuyuki Nakanishi[5], Tetsu Niwa[1,6], Thomas L. Chenevert[7], Peter R. Luijten[1], and Abass Alavi[8]

*[1]Department of Radiology, University Medical Center Utrecht, Utrecht, The Netherlands; [2]Department of Radiology, Koga Hospital 21, Kurume, Japan; [3]Department of Radiology, Royal Marsden Hospital, Sutton, United Kingdom; [4]Department of Radiology, Kobe University Graduate School of Medicine, Kobe, Japan; [5]Department of Radiology, Osaka Medical Center for Cancer and Cardiovascular Diseases, Osaka, Japan; [6]Department of Radiology, Kanagawa Children's Medical Center, Yokohama, Japan; [7]Department of Radiology, University of Michigan Medical Center, Ann Arbor, Michigan; and [8]Division of Nuclear Medicine, Hospital of the University of Pennsylvania, Philadelphia, Pennsylvania*

**Learning Objectives:** On successful completion of this activity, participants should be able to describe (1) the basic principles of DWI and (2) the current evidence on the correlation and comparison between $^{18}$F-FDG PET and DWI.

**Financial Disclosure:** The authors of this article have indicated no relevant relationships that could be perceived as a real or apparent conflict of interest.

**CME Credit:** SNM is accredited by the Accreditation Council for Continuing Medical Education (ACCME) to sponsor continuing education for physicians. SNM designates each JNM continuing education article for a maximum of 1.0 AMA PRA Category 1 Credit. Physicians should claim only credit commensurate with the extent of their participation in the activity.

For CE credit, participants can access this activity through the SNM Web site (http://www.snm.org/ce_online) through October 2011.

$^{18}$F-FDG PET is an established functional imaging modality for the evaluation of human disease. Diffusion-weighted MRI (DWI) is another rapidly evolving functional imaging modality that can be used to evaluate oncologic and nononcologic lesions throughout the body. The information provided by $^{18}$F-FDG PET and DWI can be complementary, because the 2 methods are based on completely different biophysical underpinnings. This article will describe the basic principles, clinical applications, and limitations of DWI. In addition, the available evidence that correlates and compares $^{18}$F-FDG PET and DWI will be reviewed.

**Key Words:** diffusion-weighted magnetic resonance imaging; DWI; $^{18}$F-fluoro-2-deoxyglucose; position emission tomography; FDG PET

**J Nucl Med 2010; 51:1549–1558**
DOI: 10.2967/jnumed.109.073908

PET, using the radiotracer $^{18}$F-FDG, is an established functional imaging modality for a variety of oncologic and nononcologic (e.g., inflammatory and infectious) applications (*1–3*). The contribution of $^{18}$F-FDG PET to medicine has been unmatched by any other functional imaging modality (*4*). At present, there is also growing interest in the application of diffusion-weighted MRI (DWI) in the body (*5–7*). DWI allows visualization and quantification of the mobility of water molecules and has many potential clinical applications. Importantly, although $^{18}$F-FDG PET and DWI are both functional imaging modalities and provide a high lesion-to-background contrast, they are based on completely different biophysical and biochemical underpinnings. Therefore, the information provided by the 2 imaging modalities may be regarded as complementary. Given the developing applications of DWI, the increasing use of multimodality imaging (*8*), and the expected advent of fully integrated PET/MRI systems (*9*), knowledge of the characteristics, possibilities, and limitations of DWI technique is becoming increasingly important. This is true for both the imaging specialists and the clinicians who use these modalities. This article will review the basic principles, clinical applications, and limitations of DWI. Furthermore, the available evidence that correlates and compares $^{18}$F-FDG PET with DWI will be reviewed.

Received Dec. 30, 2009; revision accepted Apr. 28, 2010.
For correspondence or reprints contact: Thomas C. Kwee, Department of Radiology, University Medical Center Utrecht, Heidelberglaan 100, 3584 CX Utrecht, The Netherlands.
E-mail: thomaskwee@gmail.com


## BASIC PRINCIPLES OF DWI

### Diffusion

DWI is sensitive to the random (Brownian) motion of water molecules. In biologic tissue, the presence of impeding barriers (e.g., cell membranes, fibers, and macromolecules) interferes with the free displacement (diffusion) of water molecules. Consequently, the signal intensity in DWI depends on the separation and permeability of these impeding boundaries (*10*). Pathologic processes that alter the physical nature of the restricting barriers in biologic tissue affect the diffusivity of the water molecules, which can be visualized and quantified using DWI (*10*). The first successful clinical application of DWI was in diagnosing

acute ischemic stroke (*11*). In acute ischemic stroke, failure of the $Na^+K^+$ adenosine triphosphatase pump leads to a net displacement of water from the extracellular to the intracellular compartment, which manifests as a precipitous drop in water mobility (*11*). However, DWI may also be useful for the evaluation of other disease processes, including oncologic and a wide variety of nononcologic (e.g., inflammatory, infectious, and traumatic) lesions (*6,11*). It is important to realize that DWI originates from T2-weighted imaging, a sequence that can detect disease because most lesions exhibit a prolonged T2 relaxation time. However, unlike T2-weighted imaging, DWI can suppress many unwanted background signals of normal structures that demonstrate perfusion, flow, or considerable diffusion (e.g., signals of gastrointestinal contents, blood vessels, and cerebrospinal fluid) and highlights lesions that exhibit impeded diffusivity. In other words, DWI detects lesions by exploiting both their prolonged T2 relaxation time and their impeded diffusivity and provides a high lesion-to-background contrast; in this respect, DWI outperforms conventional MRI sequences such as T2-weighted imaging (*5–7*). An impeded diffusivity can be encountered in 2 clinical situations. First, an increase in cellularity in tumors and cellular swelling in inflammatory or infectious lesions may lead to a decrease in extracellular volume, where increased tortuosity of the extracellular space leads to reduced water mobility. Second, abscesses and thrombi are believed to impede the diffusivity of water molecules because of their hyperviscous nature. On the other hand, necrosis and apoptotic processes may lead to loss of cell membrane integrity and a decrease in cellularity. This, in turn, increases the amount of diffusion across the cell membrane and the proportion of water molecules in the extracellular space, where water mobility is less impeded. All these processes can be evaluated using DWI.

## Development of DWI: From the Brain to the Entire Body

Until recently, the main organ of interest for DWI was the brain. Important technologic advances, including the development of echoplanar imaging, high-gradient amplitudes, multichannel coils, and parallel imaging, have extended the applications of DWI outside the brain. In particular, the introduction of parallel imaging, which allows a reduction of echo time, echo train length, and *k*-space filling time, led to substantially reduced motion artifacts and image distortions (*5–7*). Because DWI is sensitive to the motion of water molecules over a few micrometers, bulk tissue motion was initially thought to be a serious impediment when performing DWI of the chest and upper abdomen. Therefore, respiratory motion compensation techniques (i.e., breath-hold or respiration-gated acquisitions) were thought to be necessary for DWI of moving organs. However, in a breath-hold acquisition, only thick slices (typically 8–9 mm) can be obtained, limiting lesion detectability and preventing multiplanar reformats and 3-dimensional renderings. In addition, considerable scan prolongation under respiratory gating would be a serious impediment for whole-body scanning. This perceived limitation of DWI in the body has been overcome by the demonstrated feasibility of DWI under free breathing, which is also known as the concept of diffusion-weighted whole-body imaging with background body signal suppression (DWIBS) (*5–7*). Details about this concept are reported elsewhere (*7*). Advantages of DWI under free breathing over breath-hold and respiration-gated acquisitions include the possibility of obtaining thin slices (typically 4 mm) and its efficient imaging time (data can be acquired during the entire respiratory cycle). Depending on the scan parameters, a typical whole-body DWI examination can now be achieved in less than 30 min, at a clinically acceptable resolution (e.g., 160 × 256 matrix, voxel size of 2.5 × 3.6 × 4.0 mm) (*5–7*).

## Visual Resemblance Between $^{18}$F-FDG PET and DWI

$^{18}$F-FDG PET and DWIBS have visual similarities that stem from several sources. As mentioned previously, images are acquired under free breathing using the concept of DWIBS. This allows the acquisition of thin axial slices that can be used for multiplanar reformats and 3-dimensional renderings, and therefore a whole-body DWI scan can be acquired in a clinically acceptable time. Furthermore, the possibility of multiple-signal averaging is beneficial in increasing SNR, which is inherently low at higher diffusion weightings. Another important feature of this technique is the excellent suppression of unwanted background body signals by means of a fat suppression prepulse and heavy diffusion weighting (*5–7*). When applying gray-scale inversion to the obtained DWIBS dataset, a high signal intensity from low-water-mobility tissues or lesions appears in high contrast to a weak signal intensity from background tissues, resulting in images that remarkably resemble $^{18}$F-FDG PET studies (Figs. 1–6).

## Quantitative and Semiquantitative Evaluation of DWI

Diffusion in biologic tissue is quantified by means of an apparent diffusion coefficient (ADC), because the presence of natural impediments such as cell membranes, organelles, and macromolecules interferes with the free displacement of water molecules (*6,10,11*). The ADC is most frequently calculated using an implicit monoexponential model, as follows:

$$S(b)/S_0 = exp(-b \times ADC), \qquad \text{Eq. 1}$$

where $S(b)$ is the signal magnitude with diffusion weighting $b$, $S_0$ is the signal magnitude with no diffusion weighting, and $b$ is the b-value (representing the degree of diffusion weighting), which is calculated for a standard-gradient pulse pair as follows:

$$b = \gamma^2 \times G^2 \times \delta^2(\Delta - \delta/3). \qquad \text{Eq. 2}$$

Here, $\gamma$ is the gyromagnetic ratio (42.58 MHz/T for hydrogen), $G$ is the strength of the motion-probing gradients

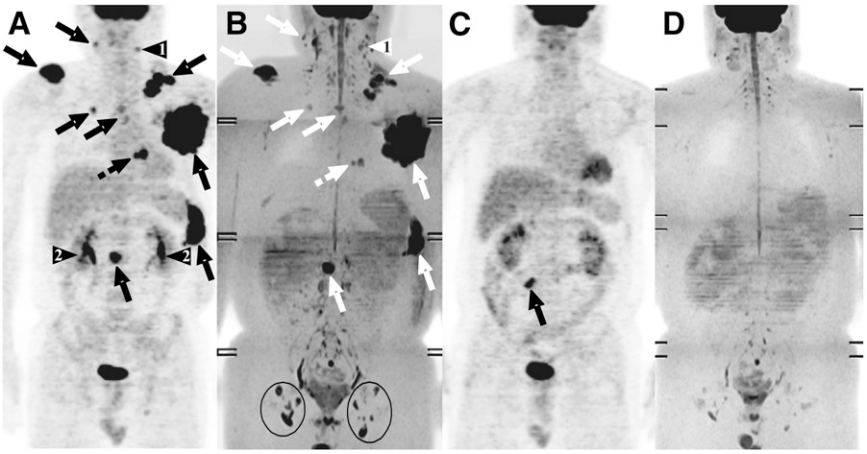


**FIGURE 1.** Comparison of pre- and postchemotherapy $^{18}$F-FDG PET and DWI in 44-y-old man with stage III diffuse large B-cell lymphoma. Coronal maximum-intensity-projection $^{18}$F-FDG PET (A) and coronal maximum-intensity-projection gray-scale inverted DWI (B) were performed before initiation of chemotherapy. Both images show cervical, bilateral supra- or infraclavicular, mediastinal, left axillary, paraaortic lymph node, and splenic involvement (solid arrows), along with cardiac involvement (dashed arrow). $^{18}$F-FDG PET (C) and DWI (D) at end of treatment show resolution of all preexisting lesions. DWI is limited in that discrimination between normal and metastatic lymph nodes is still based on size criteria; left cervical lymph node (arrowhead 1) positive on $^{18}$F-FDG PET cannot conclusively be identified as malignant on DWI. DWI also shows prominent bilateral inguinal lymph nodes (encircled), which are normal according to $^{18}$F-FDG PET. DWI, with higher spatial resolution, shows 2 separate cardiac lesions, whereas $^{18}$F-FDG PET shows only 1 large cardiac lesion. DWI also evaluates urinary tract better than does $^{18}$F-FDG PET, which can obscure potential lesions because of $^{18}$F-FDG accumulation (arrowheads 2). Physiologic $^{18}$F-FDG uptake in large intestine (arrow in C) should not be confused with persistent malignant lymphoma. (Reprinted with permission of (*7*).)

(MPGs), δ is the duration of 1 motion-probing-gradient pulse, and Δ is the interval between the leading edges of the motion-probing-gradient pulses (*6,10,11*). From Equation 1, it can be seen that at least 2 images with 2 different b-values have to be acquired to calculate an ADC. To obtain a perfusion-insensitive ADC, it is recommended to acquire the low b-value DWI dataset with a b-value of at least 100 s/mm$^2$ (*12*). The high b-value DWI dataset is often acquired using a b-value between 500 and 1,000 s/mm$^2$. For body imaging, b-values greater than 1,000 s/mm$^2$ are generally less optimal for ADC calculation because they yield inadequate SNR. It should be realized that the monoexponential ADC is only a rough approximation of the true diffusion coefficient, because diffusion exhibits multiexponential signal decay in biologic tissue (*13*). Furthermore, the use of different b-values can lead to considerable variability in the calculated monoexponential ADC (*14*). Other models, such as the biexponential model and the stretched-exponential model (*15,16*), are more suitable to describe the admixture of multiple exponential signal decays, but they require data acquisition with additional b-values (thus prolonging scan time). Moreover, multiexponential analysis routines are usually not available in standard clinical software packages. A mean ADC is most frequently used for lesion characterization, but this index may be less suitable when a lesion exhibits considerable intervoxel diffusion heterogeneity. This disadvantage can be overcome using a minimum ADC ($ADC_{min}$), an index that is thought to reflect the area with the highest cellularity (*17*). Importantly, most lesions have both an impeded diffusion and a prolonged T2 relaxation time, but the ADC does not exploit the latter for lesion characterization. Furthermore, misregistration between images with different b-values because of patient motion or image distortion may impair the reliability of ADC measurements. To overcome the limitations of the ADC, a so-called lesion–to–spinal cord ratio (LSR) was recently introduced, which is a semiquantitative measure that represents the ratio of lesion signal intensity to spinal cord signal intensity (*18*). The LSR takes into account both diffusion and T2 relaxation time, does not suffer from image misregistration issues, and has been shown to outperform the ADC in differentiating lung cancer from benign lesions (*18*). The LSR or a similar measure has the potential to replace or complement the ADC for the characterization of lesions. On the other hand, when quantitative diffusion measurements are required (e.g., in the follow-up of lesions, such as in the early prediction of response to therapy (*19–22*)), ADC measurements may still be preferred.

## CLINICAL APPLICATIONS AND LIMITATIONS OF DWI

### General Diagnostic and Prognostic Capabilities

It is beyond the scope of this paper to systematically review all applications of DWI. Rather, this section will only briefly discuss a few of the most promising clinical applications of this technique. As mentioned previously, DWI provides a high lesion-to-background contrast. Therefore, DWI is generally considered to be a sensitive imaging modality for the detection of pathology. At present, it is used mainly for the diagnosis of acute ischemic stroke (*11*). However, DWI is gaining widespread use in other areas as well (mainly oncologic), such as in liver and prostate imaging. Studies have shown that DWI is a reasonable alternative to contrast-enhanced MRI for the detection of liver metastases (*23*). Furthermore, the combination of DWI and contrast-enhanced MRI has been shown to yield the highest sensitivity without loss in specificity, compared with either of the techniques alone, for detecting liver metas-

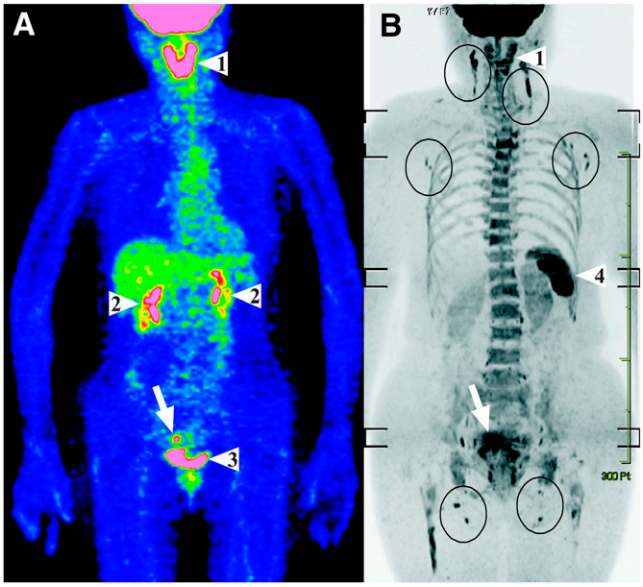


**FIGURE 2.** Comparison of $^{18}$F-FDG PET and DWI in 69-y-old-woman with pathologically proven stage IA endometrial carcinoma. Coronal maximum-intensity-projection color-scale $^{18}$F-FDG PET (A) and coronal maximum-intensity-projection gray-scale inverted DWI (B) show endometrial cancer (arrow). Relatively high $^{18}$F-FDG uptake and high signal intensity on DWI in Waldeyer ring (arrowhead 1) are not to be mistaken for disease. Furthermore, normal $^{18}$F-FDG accumulation can be seen in intrarenal collecting system and renal pelvis (arrowheads 2) and urinary bladder (arrowhead 3), potentially obscuring disease. DWI does not have this disadvantage but shows normal spleen (arrowhead 4) and several normal lymph nodes (encircled) as high-signal-intensity structures, which may limit its diagnostic performance in these organs. Red bone marrow shows normal high signal intensity on DWI.

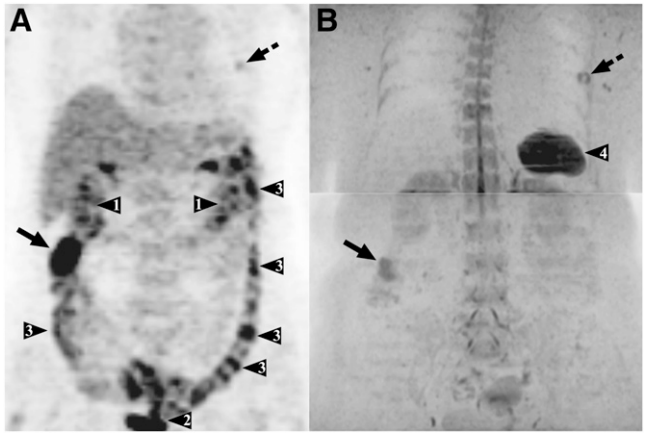


**FIGURE 3.** Comparison of $^{18}$F-FDG PET and DWI in 62-y-old woman with pathologically proven ascending colon cancer and incidentally found breast carcinoma. Both coronal maximum intensity projection $^{18}$F-FDG PET (A) and coronal maximum intensity projection gray-scale inverted DWI (B) show ascending colon cancer (solid arrows) and left-sided breast cancer (dashed arrows). Normal $^{18}$F-FDG accumulation is seen in intrarenal collecting system and renal pelvis (arrowheads 1) and urinary bladder (arrowhead 2). Normal physiologic $^{18}$F-FDG uptake in colon (arrowheads 3) may potentially obscure lesions. Delayed $^{18}$F-FDG PET may, in part, overcome this limitation. Although DWI generally does not suffer from these drawbacks, normal spleen often exhibits relatively high signal intensity on DWI (arrowhead 4), potentially obscuring disease in this organ.

tases (*24*). Other studies have shown that the combination of DWI and T2-weighted imaging is better than T2-weighted imaging alone for the detection of prostate cancer (*25,26*). Although the use of DWI in other areas is less well established, its utility for primary tumor and metastasis detection and staging in several major cancers is under active investigation (*27–33*). Because of its high lesion-to-background contrast, the additional value of DWI is expected to lie in the detection of (small) lesions that remain unnoticed on anatomic-based imaging and on functional imaging techniques with low spatial resolution such as SPECT and PET.

Another promising application is the use of quantitative DWI as a biomarker for the early assessment of response to anticancer therapy. Pretherapy ADCs in responding lesions have been reported to be significantly lower than those of nonresponding lesions in several cancers (*20–22*). The biologic basis for this finding remains unclear, but it can be speculated that a higher ADC is observed in necrotic tissue and in tissue with loss of cell membrane integrity, which may correspond to a more aggressive phenotype. It has also been reported that responding lesions show a significantly higher increase in ADC early after initiation of therapy than do nonresponding lesions (*19–22*); this finding can be attributed to changes in cell density, resulting from cytotoxic therapy–induced necrosis or apoptotic processes. More studies with larger sample sizes are required to establish the utility of this technique in predicting overall survival or long-term disease-free survival.

## Limitations

An impeded diffusion can be seen in both malignant and nonmalignant (e.g., inflammatory and infectious) lesions (*34,35*). Therefore, the specificity of DWI may be suboptimal. An impeded diffusion can also be seen in several normal structures (Table 1). It should be noted that the number and signal intensity of visualized normal tissues on DWI varies per individual and is also dependent on the applied imaging protocol. As can be seen from Table 1, the evaluation of several areas may be difficult at DWI. For example, the normal Waldeyer ring and the spleen usually have a high signal intensity on DWI (Figs. 1–3), as a result of which pathology may be obscured in these organs. Another important area in which DWI may have diagnostic difficulties is in the evaluation of lymph nodes. DWI highlights both normal and pathologic lymph nodes (Figs. 1 and 2). Normal lymph nodes already have a relatively impeded diffusion (mainly because of their high cellularity), and pathologic (e.g., malignant, inflammatory, or infected)

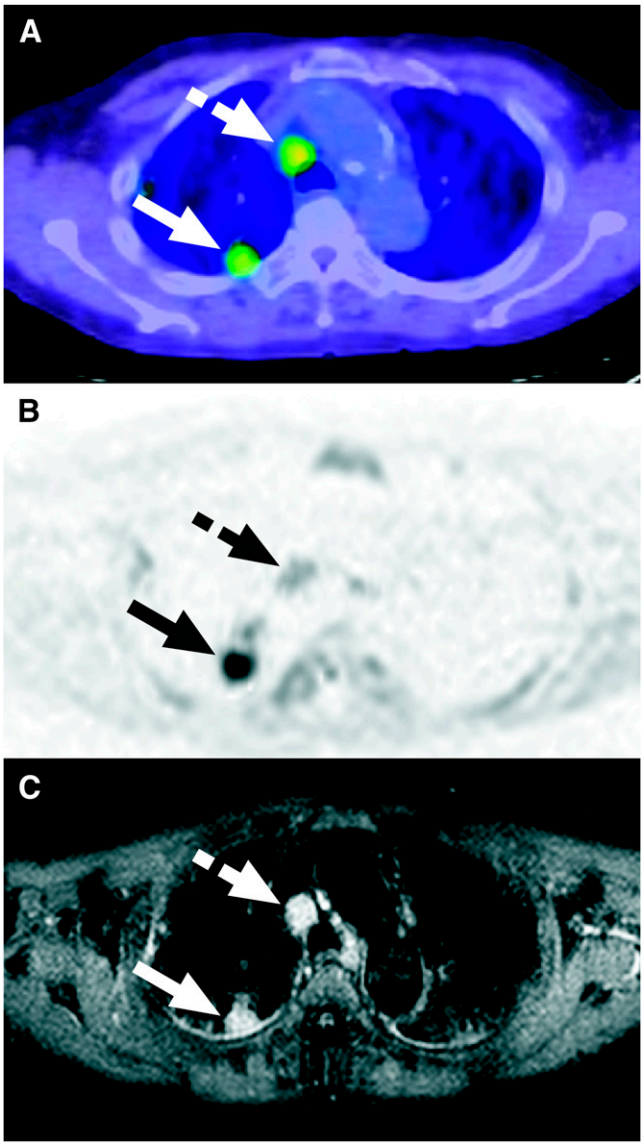


**FIGURE 4.** Comparison of $^{18}$F-FDG PET/CT, DWI, and short-inversion-time inversion recovery (STIR) in 69-y-old man with pathologically proven NSCLC and mediastinal lymph node metastasis. Axial $^{18}$F-FDG PET/CT (A) shows high $^{18}$F-FDG uptake of primary lung cancer (solid arrow) and mediastinal metastasis (dashed arrow). Axial DWI (B) clearly demonstrates primary lung cancer (solid arrow), but mediastinal lymph node metastasis exhibits only faint signal (dashed arrow), probably because of pulsatile aortic motion. STIR turbo spin-echo imaging (C) clearly shows high signal intensity of both primary lesion (solid arrow) and metastatic mediastinal lymph node (dashed arrow). Thus, conventional MRI (STIR) may increase sensitivity of DWI alone in mediastinal area.

lymph nodes may have increased cellular density or necrotic areas, further impeding or increasing diffusion, respectively. Although it has been reported that the ADCs of various causes of lymphadenopathy are significantly different from each other (*36–38*) and that the ADCs of metastatic and nonmetastatic lymph nodes may also show

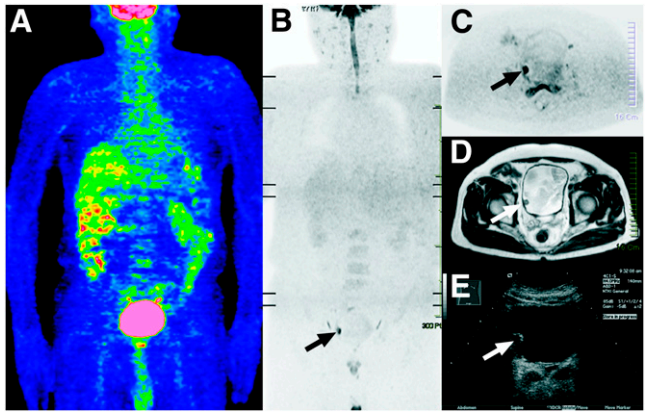


**FIGURE 5.** Comparison of $^{18}$F-FDG PET and DWI in 78-y-old man with pathologically proven stage TA urothelial cell carcinoma of urinary bladder. Coronal maximum-intensity-projection color-scale $^{18}$F-FDG PET (A) does not show urinary bladder lesion, most likely because it is obscured by normal $^{18}$F-FDG accumulation. Sagittal and axial $^{18}$F-FDG PET images (not shown) could not depict lesion either. In contrast, lesion was easily depicted on coronal limited-volume maximum-intensity-projection gray-scale inverted DWI (B, arrow). Axial gray-scale inverted DWI (C) shows that lesion in right lateral wall of urinary bladder (arrow) does not invade muscular layer. Axial T2-weighted MRI (D) and ultrasound examination (E) confirm lesion (arrows).

significant differences (*39–41*), the ADCs of normal lymph nodes and those of different nodal pathologies or conditions overlap. Furthermore, because of the susceptibility of echoplanar imaging–based DWI to image distortions, its insufficient spatial resolution, and partial-volume-averaging effects, inter- and intraobserver reproducibility in ADC measurements may be limited, causing unreliable evaluation of normal-sized lymph nodes (*42*). Combining DWI with ultrasmall superparamagnetic particles of iron oxide may improve the diagnostic perform-

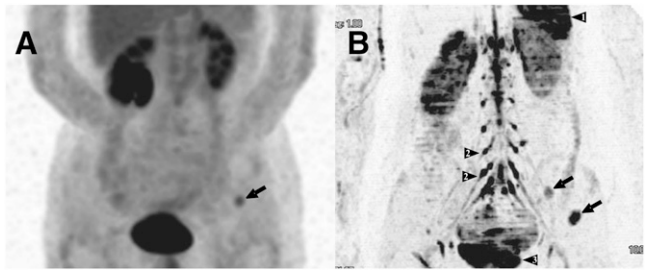


**FIGURE 6.** Comparison of $^{18}$F-FDG PET and DWI in 40-y-old woman with 2 metastatic foci in left iliac wing from breast carcinoma. Coronal maximum-intensity-projection $^{18}$F-FDG PET (A) shows only lesion (arrow), whereas coronal maximum-intensity-projection gray-scale inverted DWI (B) reveals 2 lesions in left iliac wing (arrows). Normal high signal intensity is seen in spleen (arrowhead 1), nerve roots and ganglia (arrowheads 2), and testis (arrowhead 3) on DWI.

**TABLE 1.** Visualized Normal Tissues on DWI Using b-Value of 1,000 s/mm$^2$ (Always or Commonly Seen) per Organ System

| Organ system | Structures |
|---|---|
| Nervous | Brain, spinal cord, peripheral nerves |
| Cardiovascular | — |
| Respiratory | — |
| Gastrointestinal | Salivary glands, gallbladder, small intestinal and colorectal contents |
| Lymphatic | Waldeyer ring (tonsillar and adenoidal tissue), spleen, lymph nodes |
| Genitourinary | Kidneys, adrenal glands, prostate, testis, penis, endometrium, ovaries |
| Musculoskeletal | Bone marrow |

ance of DWI alone in discriminating malignant from nonmalignant lymph nodes; this application is currently being investigated (*43*).

Another limitation of DWI is that the evaluation of structures close to the heart, such as mediastinal lymph nodes and the left liver lobe, may be compromised because of signal loss and artifacts due to severe tissue motion (*33,44–46*). Nevertheless, MRI is a versatile imaging modality, and the addition of other sequences may improve the evaluation of the mediastinal lymph nodes (*24,47*) (Fig. 4). Furthermore, combining DWI with cardiac triggering may eventually solve the problem of cardiac motion–induced signal loss.

Another drawback of DWI at high b-values is the lack of anatomic information, because signals of many normal structures are suppressed. Consequently, it may sometimes be difficult to exactly localize lesions with an impeded diffusion. The diagnostic performance of DWI alone can be improved using correlative anatomic imaging (*48*).

### Potential Complementary Roles of $^{18}$F-FDG PET and DWI

The information provided by $^{18}$F-FDG PET and DWI can be regarded as complementary, because they are based on completely different biophysical and biochemical underpinnings. For example, $^{18}$F-FDG PET may improve the evaluation of areas in which DWI often is nondiagnostic, such as structures close to the heart and the spleen. On the other hand, DWI may be of additional value to $^{18}$F-FDG PET for the evaluation of cancers that have a relatively indolent course and have associated low levels of $^{18}$F-FDG uptake, such as well-differentiated breast, lung, prostate, and neuroendocrine tumors; hepatomas; thyroid cancers; and certain types of low-grade lymphomas. Furthermore, because the attainable spatial resolution of DWI is considerably higher than that of PET, the former may detect additional lesions not seen on the latter. DWI may also be of additional value for the evaluation of areas that have normal high levels of background $^{18}$F-FDG accumulation. For example, normal $^{18}$F-FDG accumulation in the renal collecting system, ureters, and urinary bladder may obscure lesions in these locations (*49*), whereas DWI does not have this disadvantage (Fig. 5). Because $^{18}$F-FDG PET and DWI provide different biologic parameters, they may also provide valuable complementary information in the characterization of lesions and in the early assessment of anticancer therapy. However, this is still a relatively unexplored domain that requires further investigation.

## CORRELATIVE AND COMPARATIVE INVESTIGATIONS BETWEEN $^{18}$F-FDG PET AND DWI IN THE LITERATURE

### Search Strategy and Selection Criteria

PubMed was searched for studies on the correlation or comparison between $^{18}$F-FDG PET and DWI, using the search strategy as shown in Table 2. Articles were included if $^{18}$F-FDG PET and DWI were performed on the same subjects and if the same lesions were analyzed by both $^{18}$F-FDG PET and DWI. Case reports and studies investigating fewer than 25 subjects were excluded, regardless of the total number of lesions analyzed. Of 332 potentially relevant articles, 10 studies (*31,32,50–57*) fulfilled the selection criteria.

### Pulmonary Lesions and Lung Cancer

Mori et al. (*50*) prospectively performed both $^{18}$F-FDG PET and DWI on 104 patients with 140 pulmonary nodules or masses (106 malignant lesions and 34 benign lesions) within a 2-wk interval. On $^{18}$F-FDG PET, a standardized uptake value (SUV) contrast ratio between each lesion and the contralateral lung ($SUV_{CR}$) was measured, whereas on DWI, the $ADC_{min}$ of each lesion was measured, using region-of-interest analysis. $^{18}$F-FDG PET and DWI datasets were evaluated by different observers who did not know the clinical data. Of the 140 lesions, 118 were diagnosed histologically after surgical resection, whereas the other 22 were diagnosed as old inflammation because their sizes had been unchanged for more than 2 y on retrospective review of chest radiography or CT. When optimal cutoff values of $SUV_{CR}$ and $ADC_{min}$ were used for benign–malignant discrimination, as determined by receiver operating characteristic (ROC) analysis, the sensitivities of $SUV_{CR}$ and $ADC_{min}$ measurements (70% and 72%, respectively)

**TABLE 2.** Search Strategy and Results from PubMed as of December 12, 2009

| Step | Search string | No. of articles |
|---|---|---|
| 1 | Fluorodeoxyglucose OR 2-fluoro-2-deoxy-d-glucose OR FDG OR PET OR Positron emission tomography OR PET | 48,943 |
| 2 | Magnetic resonance OR MR imaging OR MRI OR Magnetic resonance tomography OR Nuclear magnetic resonance OR NMR | 433,871 |
| 3 | Diffusion | 109,642 |
| 4 | Step 1 AND 2 AND 3 | 355 |

were not significantly different ($P = 0.85$). On the other hand, the specificity of $ADC_{min}$ measurements (97%) was significantly higher ($P = 0.03$) than that of $SUV_{CR}$ measurements (79%), as was attributable to the fact that the former produced fewer false-positive results for active inflammation than did the latter. Although the authors concluded that DWI may be used instead of $^{18}$F-FDG PET to distinguish malignant from benign pulmonary nodules or masses with fewer false-positive results, cutoff $SUV_{CR}$ and $ADC_{min}$ values were determined by applying post hoc analysis of the obtained data and may have inflated the accuracy of both $SUV_{CR}$ and $ADC_{min}$ measurements. Mori et al. also reported that $SUV_{CR}$ and $ADC_{min}$ were inversely correlated ($R = -0.504$, $P < 0.001$). However, the clinical implications of this correlation were not investigated.

Ohba et al. (*51*) examined whether DWI might be as useful as $^{18}$F-FDG PET for discriminating between non–small cell lung cancer (NSCLC) and benign pulmonary nodules and for predicting the aggressiveness of NSCLC. A total of 110 patients who had 124 pulmonary nodules smaller than 3 cm (96 NSCLCs and 28 benign nodules) and had undergone both $^{18}$F-FDG PET and DWI within a 2-wk interval were retrospectively assessed. $ADC_{min}$ and $SUV_{CR}$ measurements were done and analyzed as described previously (*50*). In addition, the $ADC_{min}$ and the $SUV_{CR}$ were compared between pathologic stage IA and stage IB or more advanced stages; between tumors with and without lymphatic, vascular, or pleural involvement; and between well-differentiated and moderately or poorly differentiated adenocarcinomas. Of the 124 nodules, 106 were diagnosed histologically after surgical resection, whereas 18 were diagnosed as old inflammation because their sizes were found on retrospective review of chest radiography or CT to have been unchanged for more than 2 y. Using optimal cutoff values of $SUV_{CR}$ and $ADC_{min}$ for benign–malignant discrimination, as determined by means of ROC analysis, it was shown that the sensitivity and specificity of $SUV_{CR}$ measurements (72% and 82%, respectively) were not significantly different ($P > 0.999$ and $P = 0.22$, respectively) from those of $ADC_{min}$ measurements (73% and 96%, respectively). Furthermore, unlike $ADC_{min}$ measurements, $SUV_{CR}$ measurements were significantly different between NSCLC at pathologic stage IA and IB or more advanced stages; between NSCLC with and without lymphatic, vascular, and pleural involvements; and between well-differentiated and moderately or poorly differentiated adenocarcinomas ($P <$ 0.01–0.001). The authors concluded that although DWI can assess NSCLC as well as $^{18}$F-FDG PET does, it cannot predict the aggressiveness of NSCLC (in particular of adenocarcinoma). However, study limitations include possible selection bias due to the retrospective nature of the research and the fact that optimal cutoff values of $SUV_{CR}$ and $ADC_{min}$ were obtained by means of post hoc analysis of the obtained data. Setting cutoff values to optimize discrimination and then applying them to the same data from which they were derived is rarely of real clinical value, because these cutoff values will be applied to novel (different) datasets in which they will most likely yield a lower diagnostic performance.

Kanauchi et al. (*52*), to assess the role of DWI for predicting tumor invasiveness, investigated 41 patients with clinical stage IA NSCLC who underwent both $^{18}$F-FDG PET/CT and DWI. A previous study had already shown that the maximum SUV ($SUV_{max}$) is an independent predictor of disease-free survival in NSCLC (*58*). All tumors in the study of Kanauchi et al. were surgically resected and histopathologically examined. Lung cancers that exhibited nodal, lymphovascular, or pleural invasion were defined as invasive. Nodules with low signal intensity on DWI, comparable to or even lower than that of the spinal cord (i.e., LSR $\geq 1$), were classified as positive on DWI. Otherwise, they were considered negative on DWI. The $SUV_{max}$ of DWI-positive patients ($10.33 \pm 4.93$) was significantly higher ($P < 0.001$) than that of DWI-negative patients ($3.10 \pm 4.21$). Furthermore, multivariate analysis (excluding $SUV_{max}$) showed that DWI was a significant independent predictive factor for invasive cancer ($P =$ 0.005). The sensitivity of DWI for prediction of tumor invasiveness was 90%, its specificity was 81%, its positive predictive value was 60.0%, and its negative predictive value was 96%. On the basis of these findings, the authors speculated that, unlike the ADC (*50*), the LSR might be a useful method for predicting tumor invasiveness in clinical stage IA NSCLC. On the other hand, the results of this study should be interpreted with caution, because it was not clear whether patients were prospectively or retrospectively included, the time interval between $^{18}$F-FDG PET/CT and DWI was not described, and it was unclear whether $^{18}$F-FDG PET/CT and DWI were separately evaluated without knowledge of the findings of the other imaging modality and without knowledge of histopathologic findings.

Nomori et al. (*53*) prospectively compared $^{18}$F-FDG PET/CT and DWI for N-staging in 88 patients with NSCLC who were scheduled to undergo pulmonary resection and mediastinal lymph node dissection. On $^{18}$F-FDG PET, a contrast ratio between each lymph node with a long axis of more than 1 cm and the cerebellum ($SUV_{CR}$) was measured, whereas on DWI, the $ADC_{min}$ of each lesion was measured, using region-of-interest analysis. $^{18}$F-FDG PET and DWI datasets were evaluated by different observers. The specificity of DWI for N-staging was significantly higher ($P = 0.002$) than that of $^{18}$F-FDG PET/CT. These findings were attributable to the fact that DWI produced fewer false-positive results for lymphadenitis than did $^{18}$F-FDG PET/CT. Nonetheless, DWI was false-positive in a few cases with granulation tissue in tuberculous or nontuberculous lymph nodes. Nomori et al. concluded that DWI can be used instead of $^{18}$F-FDG PET/CT for N-staging of NSCLC, with fewer false-positive results than are obtained with $^{18}$F-FDG PET/CT. Nevertheless, the study of Nomori et al. suffered from the same limitations as those

described previously for Mori et al. (*50*), most likely because both studies used almost the same series of patients. Furthermore, Nomori et al. failed to mention the interval between $^{18}$F-FDG PET and DWI, and it was not stated whether $^{18}$F-FDG PET and DWI datasets were separately evaluated without knowledge of the findings of the other imaging modality and without knowledge of histopathologic findings. In addition, the results of Nomori et al. are applicable only to lymph nodes with a long-axis diameter of more than 1 cm.

Ohno et al. (*31*) prospectively compared whole-body DWI alone, whole-body DWI combined with conventional whole-body MRI, and $^{18}$F-FDG PET/CT for M-stage assessment in 203 NSCLC patients. All studies were performed in random order within 3 wk of diagnosis and before treatment. Masked MRI and $^{18}$F-FDG PET/CT datasets were qualitatively assessed by different observers. The final M-stage and metastasis of a given site were determined on the basis of the results of conventional radiologic, $^{18}$F-FDG PET/CT, and whole-body MRI examinations and on the basis of pathologic results from endoscopic, CT-guided, or surgical biopsies, as well as on the basis of the results of follow-up examinations performed on every patient for more than 12 mo. The area under the ROC curve of whole-body DWI (0.79) was significantly lower ($P < 0.05$) than that of $^{18}$F-FDG PET/CT (0.89). However, the area under the curve of whole-body DWI combined with conventional whole-body MRI (0.87) was not significantly different from that of $^{18}$F-FDG PET/CT. The authors concluded that whole-body MRI with DWI can be used for M-stage assessment in patients with NSCLC with an accuracy as good as that of $^{18}$F-FDG PET/CT. This well-designed study has only some minor limitations, among which were the facts that histopathologic results were (inevitably) not available for every patient and that diagnostic performance on a per-site basis was not assessed.

Takenaka et al. (*32*) prospectively compared the diagnostic performance of whole-body DWI alone and whole-body DWI combined with conventional whole-body MRI to $^{18}$F-FDG PET/CT with respect to bone marrow metastasis assessment in 115 patients with NSCLC. All studies were performed in random order within 3 wk of diagnosis and before treatment. Masked MRI and $^{18}$F-FDG PET/CT datasets were qualitatively assessed by different observers. The reference standard was based on the results of initial and follow-up bone scintigraphy, integrated $^{18}$F-FDG PET/CT, and whole-body MRI examinations and pathologic examinations from CT-guided or surgical biopsies ($n = 52$ sites), as well as of follow-up examinations for more than 12 mo ($n = 973$ sites) for every patient. On both a per-site and a per-patient basis, the sensitivities of whole-body DWI alone and whole-body DWI combined with conventional whole-body MRI were not significantly different ($P > 0.05$) from those of $^{18}$F-FDG PET/CT. However, on both a per-site and a per-patient basis, the specificities of whole-body DWI alone (93.7% and 78.9%, respectively) were significantly lower ($P < 0.05$) than those of $^{18}$F-FDG PET/CT (95.4% and 85.6%, respectively). On the other hand, the specificity on a per-site basis of the combination of whole-body DWI with conventional whole-body MRI was significantly higher ($P < 0.05$) than that of $^{18}$F-FDG PET/CT (95.4%), with no significant differences in specificity ($P > 0.05$) on a per-patient basis between the 2 modalities. Takenaka et al. concluded that whole-body MRI with DWI is more specific for bone marrow assessment in patients with NSCLC than is $^{18}$F-FDG PET/CT. In addition, the use of whole-body DWI as an adjunct to whole-body MRI without whole-body DWI can improve the sensitivity of the whole-body MRI examination. The limitations of this study are similar to those previously described for the study of Ohno et al. (*31*), given the similarities in study design.

### Colorectal Cancer

Ono et al. (*54*) aimed to compare DWI with $^{18}$F-FDG PET regarding detection of the primary tumor and detection of lymph node metastases in patients with colorectal cancer. A total of 25 patients who had 27 surgically proven colorectal lesions and had undergone both DWI and $^{18}$F-FDG PET were retrospectively reviewed. DWI and $^{18}$F-FDG PET were performed within 9 d. Masked DWI and $^{18}$F-FDG PET datasets were qualitatively assessed by different observers. Diffusion-weighted images were interpreted in combination with T2-weighted images. For the interpretation of $^{18}$F-FDG PET images, CT or ultrasound images provided an anatomic reference. Of the 27 primary colorectal lesions surgically excised, 23 (85.2%) were true-positive on both DWI and $^{18}$F-FDG PET. Two lesions were false-negative on DWI but true-positive on $^{18}$F-FDG PET, and 2 were false-negative on both DWI and $^{18}$F-FDG PET. With respect to metastatic lymph node detection, DWI and $^{18}$F-FDG PET had sensitivities of 80% (8/10) and 30.0% (3/10), respectively, and specificities of 76.9% (10/13) and 100% (13/13), respectively. Ono et al. stated that their initial results may suggest that DWI is inferior to $^{18}$F-FDG PET for the detection of primary colorectal cancer but superior for the detection of lymph node metastases. However, important limitations of the study of Ono et al. are its retrospective design, the small number of patients, and the fact that the observers knew that all patients had a histopathologic diagnosis of colorectal cancer.

### Uterine Cervical Cancer

Choi et al. (*55*) retrospectively investigated 236 patients with uterine cervical cancer who had undergone both DWI and $^{18}$F-FDG PET/CT within a 2-wk interval. Only 1 "representative" lymph node with a short-axis diameter of 5 mm or greater on T2-weighted images was selected per lymph node station. Mean ADC and $ADC_{min}$ of selected lymph nodes were measured by an observer who was masked to the $^{18}$F-FDG PET/CT findings. $^{18}$F-FDG PET/CT findings were used as the standard of reference. Both mean ADC and $ADC_{min}$ (in $10^{-3}$ mm$^2$/s) in $^{18}$F-FDG PET/CT–positive lymph nodes ($0.756 \pm 0.172$ and $0.6436 \pm 0.1348$, respec-

tively) were significantly lower ($P < 0.001$) than those of $^{18}$F-FDG PET/CT–negative lymph nodes (1.019 ± 0.238 and 0.8893 ± 0.2074, respectively). The area under the curve of $ADC_{min}$ (0.864) was significantly higher ($P = 0.014$) that that of mean ADC (0.836). The use of an optimal cutoff value of $ADC_{min}$ yielded a sensitivity of 86%, a specificity of 80%, a positive predictive value of 69%, and a negative predictive value of 91%. Despite the fact that the study was retrospective, included only lymph nodes with a short-axis diameter of 5 mm or greater, used post hoc determination of an optimal cutoff value, and lacked histopathologic correlation, the results suggest a good correlation between DWI with ADC measurements and $^{18}$F-FDG PET/CT in nodal characterization.

Ho et al. (*56*) retrospectively assessed 33 patients with uterine cervical cancer who had undergone both $^{18}$F-FDG PET and DWI within a 2-wk interval. Regions of interest were drawn on the primary tumor on $^{18}$F-FDG PET and diffusion-weighted images to calculate SUV and ADC indices, respectively. The relative $ADC_{min}$, defined as the ratio of $ADC_{min}$ to mean ADC, was significantly inversely correlated in all study patients with the relative $SUV_{max}$, defined as the ratio of $SUV_{max}$ to mean SUV ($R = –0.526$, $P = 0.0017$). A significantly inverse correlation between relative $ADC_{min}$ and relative $SUV_{max}$ was observed in patients with adenocarcinoma or adenosquamous carcinoma ($R = –0.685$, $P = 0.0012$) and those with well- to moderately differentiated tumor ($R = –0.631$, $P = 0.0050$). No significant correlation was demonstrated in patients with squamous cell carcinoma or poorly differentiated tumor. The authors concluded that the significantly inverse correlation between relative $ADC_{min}$ and relative $SUV_{max}$ in primary cervical tumor suggests that DWI and $^{18}$F-FDG PET/CT might play a complementary role for the clinical assessment of this cancer type. Unfortunately, the clinical implications of this correlation were not explored. This study was also limited by its retrospective design, the low number of patients, and the fact that it was not explicitly stated whether $^{18}$F-FDG PET and DWI datasets were separately evaluated without knowledge of the findings of the other imaging modality.

### General Whole-Body Oncologic Imaging

Stecco et al. (*57*) prospectively compared whole-body DWI to $^{18}$F-FDG PET/CT for staging of 29 oncologic patients (malignant lymphoma: $n = 15$; lung cancer: $n = 3$; breast cancer: $n = 3$; gastrointestinal cancer: $n = 3$; kidney cancer: $n = 2$; sarcoma: $n = 1$, primitive neuroectodermal tumor: $n = 1$; prostate cancer: $n = 1$). Whole-body DWI was evaluated by 2 independent observers who were masked to the $^{18}$F-FDG PET/CT findings. $^{18}$F-FDG PET/CT was evaluated by another observer. Whole-body DWI and $^{18}$F-FDG PET datasets were assessed according to 40 predefined skeletal and visceral sites and subsites. Using $^{18}$F-FDG PET/CT results as the standard of reference, whole-body DWI had region-based sensitivities of 89.1% (106/119) and 87.4% (104/119), specificities of 98.5% (1,183/1,201) and 98.8% (1,187/1,201), and accuracies of 97.7% (1,289/1,320) and 97.8% (1,291/1,320) for readers 1 and 2, respectively. The authors concluded that whole-body DWI provided a high specificity and negative predictive value. Limitations of this study are the small size and heterogeneity of the patient population, the use of a suboptimal DWI protocol that yielded suboptimal image quality (an integrated body coil was used instead of surface coils with parallel imaging capabilities), and the fact that $^{18}$F-FDG PET/CT itself is an imperfect reference standard.

## CONCLUSION

DWI is emerging as a promising functional whole-body imaging modality that may eventually become complementary to $^{18}$F-FDG PET in several clinical applications. Studies on the correlation and comparison between $^{18}$F-FDG PET and DWI are still scarce, and most of these studies suffer from several methodologic shortcomings. Future well-designed prospective studies in various clinical settings and in different institutions are necessary to provide more insight into the advantages and disadvantages of DWI, compared with $^{18}$F-FDG PET, in terms of patient tolerance and safety aspects, diagnostic and prognostic capabilities, and cost-effectiveness.

## REFERENCES


1. Alavi A, Reivich M. Guest editorial: the conception of FDG-PET imaging. *Semin Nucl Med.* 2002;32:2–5.
2. Fletcher JW, Djulbegovic B, Soares HP, et al. Recommendations on the use of $^{18}$F-FDG PET in oncology. *J Nucl Med.* 2008;49:480–508.
3. Basu S, Chryssikos T, Moghadam-Kia S, Zhuang H, Torigian DA, Alavi A. Positron emission tomography as a diagnostic tool in infection: present role and future possibilities. *Semin Nucl Med.* 2009;39:36–51.
4. Basu S, Alavi A. Unparalleled contribution of $^{18}$F-FDG PET to medicine over 3 decades. *J Nucl Med.* 2008;49(10):17N–21N, 37N.
5. Takahara T, Imai Y, Yamashita T, Yasuda S, Nasu S, Van Cauteren M. Diffusion weighted whole body imaging with background body signal suppression (DWIBS): technical improvement using free breathing, STIR and high resolution 3D display. *Radiat Med.* 2004;22:275–282.
6. Koh DM, Collins DJ. Diffusion-weighted MRI in the body: applications and challenges in oncology. *AJR.* 2007;188:1622–1635.
7. Kwee TC, Takahara T, Ochiai R, Nievelstein RA, Luijten PR. Diffusion-weighted whole-body imaging with background body signal suppression (DWIBS): features and potential applications in oncology. *Eur Radiol.* 2008; 18:1937–1952.
8. Bischof Delaloye A, Carrió I, Cuocolo A, et al. White paper of the European Association of Nuclear Medicine (EANM) and the European Society of Radiology (ESR) on multimodality imaging. *Eur J Nucl Med Mol Imaging.* 2007;34:1147–1151.
9. Pichler BJ, Kolb A, Nägele T, Schlemmer HP. PET/MRI: paving the way for the next generation of clinical multimodality imaging applications. *J Nucl Med.* 2010;51:333–336.
10. Sotak CH. Nuclear magnetic resonance (NMR) measurement of the apparent diffusion coefficient (ADC) of tissue water and its relationship to cell volume changes in pathological states. *Neurochem Int.* 2004;45:569–582.
11. Schaefer PW, Grant PE, Gonzalez RG. Diffusion-weighted MR imaging of the brain. *Radiology.* 2000;217:331–345.
12. Padhani AR, Liu G, Koh DM, et al. Diffusion-weighted magnetic resonance imaging as a cancer biomarker: consensus and recommendations. *Neoplasia.* 2009;11:102–125.
13. Lee JH, Springer CS Jr. Effects of equilibrium exchange on diffusion-weighted NMR signals: the diffusigraphic "shutter-speed." *Magn Reson Med.* 2003;49: 450–458.

14. Zhang JL, Sigmund EE, Chandarana H, et al. Variability of renal apparent diffusion coefficients: limitations of the monoexponential model for diffusion quantification. *Radiology.* 2010;254:783–792.
15. Maier SE, Bogner P, Bajzik G, et al. Normal brain and brain tumor: multicomponent apparent diffusion coefficient line scan imaging. *Radiology.* 2001;219:842–849.
16. Bennett KM, Schmainda KM, Bennett RT, Rowe DB, Lu H, Hyde JS. Characterization of continuously distributed cortical water diffusion rates with a stretched-exponential model. *Magn Reson Med.* 2003;50:727–734.
17. Sugahara T, Korogi Y, Kochi M, et al. Usefulness of diffusion-weighted MRI with echo-planar technique in the evaluation of cellularity in gliomas. *J Magn Reson Imaging.* 1999;9:53–60.
18. Uto T, Takehara Y, Nakamura Y, et al. Higher sensitivity and specificity for diffusion-weighted imaging of malignant lung lesions without apparent diffusion coefficient quantification. *Radiology.* 2009;252:247–254.
19. Hamstra DA, Galbán CJ, Meyer CR, et al. Functional diffusion map as an early imaging biomarker for high-grade glioma: correlation with conventional radiologic response and overall survival. *J Clin Oncol.* 2008;26:3387–3394.
20. Kim S, Loevner L, Quon H, et al. Diffusion-weighted magnetic resonance imaging for predicting and detecting early response to chemoradiation therapy of squamous cell carcinomas of the head and neck. *Clin Cancer Res.* 2009; 15:986–994.
21. Cui Y, Zhang XP, Sun YS, Tang L, Shen L. Apparent diffusion coefficient: potential imaging biomarker for prediction and early detection of response to chemotherapy in hepatic metastases. *Radiology.* 2008;248:894–900.
22. Liu Y, Bai R, Sun H, Liu H, Zhao X, Li Y. Diffusion-weighted imaging in predicting and monitoring the response of uterine cervical cancer to combined chemoradiation. *Clin Radiol.* 2009;64:1067–1074.
23. Hardie AD, Naik M, Hecht EM, et al. Diagnosis of liver metastases: value of diffusion-weighted MRI compared with gadolinium-enhanced MRI. *Eur Radiol.* 2010;20:1431–1441.
24. Koh DM, Brown G, Riddell AM, et al. Detection of colorectal hepatic metastases using MnDPDP MR imaging and diffusion-weighted imaging (DWI) alone and in combination. *Eur Radiol.* 2008;18:903–910.
25. Haider MA, van der Kwast TH, Tanguay J, et al. Combined T2-weighted and diffusion-weighted MRI for localization of prostate cancer. *AJR.* 2007;189: 323–328.
26. Lim HK, Kim JK, Kim KA, Cho KS. Prostate cancer: apparent diffusion coefficient map with T2-weighted images for detection—a multireader study. *Radiology.* 2009;250:145–151.
27. Ichikawa T, Erturk SM, Motosugi U, et al. High-B-value diffusion-weighted MRI in colorectal cancer. *AJR.* 2006;187:181–184.
28. Ichikawa T, Erturk SM, Motosugi U, et al. High-b value diffusion-weighted MRI for detecting pancreatic adenocarcinoma: preliminary results. *AJR.* 2007;188: 409–414.
29. Inada Y, Matsuki M, Nakai G, et al. Body diffusion-weighted MR imaging of uterine endometrial cancer: is it helpful in the detection of cancer in nonenhanced MR imaging? *Eur J Radiol.* 2009;70:122–127.
30. Nakanishi K, Kobayashi M, Nakaguchi K, et al. Whole-body MRI for detecting metastatic bone tumor: diagnostic value of diffusion-weighted images. *Magn Reson Med Sci.* 2007;6:147–155.
31. Ohno Y, Koyama H, Onishi Y, et al. Non-small cell lung cancer: whole-body MR examination for M-stage assessment—utility for whole-body diffusion-weighted imaging compared with integrated FDG PET/CT. *Radiology.* 2008;248:643–654.
32. Takenaka D, Ohno Y, Matsumoto K, et al. Detection of bone metastases in non-small cell lung cancer patients: comparison of whole-body diffusion-weighted imaging (DWI), whole-body MR imaging without and with DWI, whole-body FDG-PET/CT, and bone scintigraphy. *J Magn Reson Imaging.* 2009;30: 298–308.
33. Kwee TC, Quarles van Ufford HM, Beek FJ, et al. Whole-body MRI, including diffusion-weighted imaging, for the initial staging of malignant lymphoma: comparison to computed tomography. *Invest Radiol.* 2009;44:683–690.
34. Humphries PD, Sebire NJ, Siegel MJ, Olsen ØE. Tumors in pediatric patients at diffusion-weighted MR imaging: apparent diffusion coefficient and tumor cellularity. *Radiology.* 2007;245:848–854.
35. Feuerlein S, Pauls S, Juchems MS, et al. Pitfalls in abdominal diffusion-weighted imaging: how predictive is restricted water diffusion for malignancy. *AJR.* 2009;193:1070–1076.
36. Sumi M, Sakihama N, Sumi T, et al. Discrimination of metastatic cervical lymph nodes with diffusion-weighted MR imaging in patients with head and neck cancer. *AJNR.* 2003;24:1627–1634.
37. Sumi M, Van Cauteren M, Nakamura T. MR microimaging of benign and malignant nodes in the neck. *AJR.* 2006;186:749–757.
38. King AD, Ahuja AT, Yeung DK, et al. Malignant cervical lymphadenopathy: diagnostic accuracy of diffusion-weighted MR imaging. *Radiology.* 2007; 245:806–813.
39. Kim JK, Kim KA, Park BW, Kim N, Cho KS. Feasibility of diffusion-weighted imaging in the differentiation of metastatic from nonmetastatic lymph nodes: early experience. *J Magn Reson Imaging.* 2008;28:714–719.
40. Park SO, Kim JK, Kim KA, et al. Relative apparent diffusion coefficient: determination of reference site and validation of benefit for detecting metastatic lymph nodes in uterine cervical cancer. *J Magn Reson Imaging.* 2009;29:383–390.
41. Vandecaveye V, De Keyzer F, Vander Poorten V, et al. Head and neck squamous cell carcinoma: value of diffusion-weighted MR imaging for nodal staging. *Radiology.* 2009;251:134–146.
42. Kwee TC, Takahara T, Luijten PR, Nievelstein RA. ADC measurements of lymph nodes: inter- and intra-observer reproducibility study and an overview of the literature. *Eur J Radiol*. April 15, 2009 [Epub ahead of print].
43. Thoeny HC, Triantafyllou M, Birkhaeuser FD, et al. Combined ultrasmall superparamagnetic particles of iron oxide-enhanced and diffusion-weighted magnetic resonance imaging reliably detect pelvic lymph node metastases in normal-sized nodes of bladder and prostate cancer patients. *Eur Urol.* 2009; 55:761–769.
44. Sakurada A, Takahara T, Kwee TC, et al. Diagnostic performance of diffusion-weighted magnetic resonance imaging in esophageal cancer. *Eur Radiol.* 2009; 19:1461–1469.
45. Nasu K, Kuroki Y, Sekiguchi R, Kazama T, Nakajima H. Measurement of the apparent diffusion coefficient in the liver: is it a reliable index for hepatic disease diagnosis? *Radiat Med.* 2006;24:438–444.
46. Kwee TC, Takahara T, Niwa T, et al. Influence of cardiac motion on diffusion-weighted magnetic resonance imaging of the liver. *MAGMA.* 2009;22:319–325.
47. Ohno Y, Koyama H, Nogami M, et al. STIR turbo SE MR imaging vs. coregistered FDG-PET/CT: quantitative and qualitative assessment of N-stage in non-small-cell lung cancer patients. *J Magn Reson Imaging.* 2007;26:1071–1080.
48. Tsushima Y, Takano A, Taketomi-Takahashi A, Endo K. Body diffusion-weighted MR imaging using high b-value for malignant tumor screening: usefulness and necessity of referring to T2-weighted images and creating fusion images. *Acad Radiol.* 2007;14:643–650.
49. Cook GJ, Fogelman I, Maisey MN. Normal physiological and benign pathological variants of 18-fluoro-2-deoxyglucose positron-emission tomography scanning: potential for error in interpretation. *Semin Nucl Med.* 1996;26:308–314.
50. Mori T, Nomori H, Ikeda K, et al. Diffusion-weighted magnetic resonance imaging for diagnosing malignant pulmonary nodules/masses: comparison with positron emission tomography. *J Thorac Oncol.* 2008;3:358–364.
51. Ohba Y, Nomori H, Mori T, et al. Is diffusion-weighted magnetic resonance imaging superior to positron emission tomography with fludeoxyglucose F 18 in imaging non-small cell lung cancer? *J Thorac Cardiovasc Surg.* 2009;138: 439–445.
52. Kanauchi N, Oizumi H, Honma T, et al. Role of diffusion-weighted magnetic resonance imaging for predicting of tumor invasiveness for clinical stage IA non-small cell lung cancer. *Eur J Cardiothorac Surg.* 2009;35: 706–710.
53. Nomori H, Mori T, Ikeda K, et al. Diffusion-weighted magnetic resonance imaging can be used in place of positron emission tomography for N staging of non-small cell lung cancer with fewer false-positive results. *J Thorac Cardiovasc Surg.* 2008;135:816–822.
54. Ono K, Ochiai R, Yoshida T, et al. Comparison of diffusion-weighted MRI and 2-[fluorine-18]-fluoro-2-deoxy-D-glucose positron emission tomography (FDG-PET) for detecting primary colorectal cancer and regional lymph node metastases. *J Magn Reson Imaging.* 2009;29:336–340.
55. Choi EK, Kim JK, Choi HJ, et al. Node-by-node correlation between MR and PET/CT in patients with uterine cervical cancer: diffusion-weighted imaging versus size-based criteria on T2WI. *Eur Radiol.* 2009;19:2024–2032.
56. Ho KC, Lin G, Wang JJ, Lai CH, Chang CJ, Yen TC. Correlation of apparent diffusion coefficients measured by 3T diffusion-weighted MRI and SUV from FDG PET/CT in primary cervical cancer. *Eur J Nucl Med Mol Imaging.* 2009;36:200–208.
57. Stecco A, Romano G, Negru M, et al. Whole-body diffusion-weighted magnetic resonance imaging in the staging of oncological patients: comparison with positron emission tomography computed tomography (PET-CT) in a pilot study. *Radiol Med (Torino).* 2009;114:11–17.
58. Higashi K, Ueda Y, Arisaka Y, et al. $^{18}$F-FDG uptake as a biologic prognostic factor for recurrence in patients with surgically resected non-small cell lung cancer. *J Nucl Med.* 2002;43:39–45.